Monthly Notices
of the
ROYAL ASTRONOMICAL SOCIETY

Mon. Not. R. Astron. Soc. **424,** 1930–1940 (2012) doi:10.1111/j.1365-2966.2012.21322.x

Oxygen and nitrogen abundances of H II regions in six spiral galaxies

A. S. Gusev,[1⋆] L. S. Pilyugin,[2] F. Sakhibov,[3] S. N. Dodonov,[4] O. V. Ezhkova[1] and M. S. Khramtsova[5]

[1] *Sternberg Astronomical Institute, Lomonosov Moscow State University, Universitetsky pr. 13, 119992 Moscow, Russia*
[2] *Main Astronomical Observatory of National Academy of Sciences of Ukraine, Zabolotnogo str. 27, 03680 Kiev, Ukraine*
[3] *University of Applied Sciences of Mittelhessen, Campus Friedberg, Department of Mathematics, Natural Sciences and Data Processing, Wilhelm-Leuschner-Strasse 13, 61169 Friedberg, Germany*
[4] *Special Astrophysical Observatory, Russian Academy of Sciences, 369169 Nizhnij Arkhyz, Russia*
[5] *Institute of Astronomy, Russian Academy of Sciences, ul. Pyatnitskaya 48, 119017 Moscow, Russia*

Accepted 2012 May 15. Received 2012 May 14; in original form 2012 February 29

ABSTRACT

Spectroscopic observations of 63 H II regions in six spiral galaxies (NGC 628, NGC 783, NGC 2336, NGC 6217, NGC 7331 and NGC 7678) were carried out with the 6-m telescope (BTA) of Russian Special Astrophysical Observatory with the Spectral Camera attached to the focal reducer SCORPIO in multislit mode with a dispersion of 2.1 Å pixel^{-1} and a spectral resolution of 10 Å. These observations were used to estimate the oxygen and nitrogen abundances and the electron temperatures in H II regions through the recent variant of the strong-line method (NS calibration). The parameters of the radial distribution (the extrapolated central intercept value and the gradient) of the oxygen and nitrogen abundances in the discs of spiral galaxies NGC 628, NGC 783, NGC 2336, NGC 7331 and NGC 7678 have been determined. The abundances in NGC 783, NGC 2336, NGC 6217 and NGC 7678 are measured for the first time. Galaxies from our sample follow well the general trend in the luminosity–central metallicity diagram for spiral and irregular galaxies.

Key words: techniques: spectroscopic – ISM: abundances – H II regions – galaxies: abundances.

1 INTRODUCTION

We have observed emission-line spectra of 63 giant H II regions in six spiral galaxies as part of our study of star-formation regions in spiral and irregular galaxies. Giant extragalactic H II regions are the birthplaces of star clusters and can be used to study the current star formation and chemical abundances in galaxies. Giant H II regions are ionized by clusters of young massive stars. Their sizes range from several tens to ≈500 pc, so they are larger and brighter in comparison with Galactic H II regions. Certain selection effects must be noted. Necessarily poorer spatial resolution contributes to a tendency to identify larger regions in more distant galaxies; at better resolution these regions break up into groups or chains of smaller clumps (Dinerstein 1990).

One of the main interests in H II regions is the study of elemental abundances and their gradients in galaxies. A large number of regions have been observed for this purpose (Zaritsky, Kennicutt & Huchra 1994; Roy et al. 1996; van Zee et al. 1998; Dutil & Roy 1999; Kennicutt, Bresolin & Garnett 2003; Bresolin et al. 2005, 2009, among others). Radial distributions of oxygen and nitrogen abundances across the discs are mandatory in investigations of different aspects of formation and evolution of spiral galaxies. The measurement of the distribution of elemental abundances within galaxies is a tool for studying galaxy formation and evolution. There are several investigations of possible relationships between the abundance properties and global characteristics of galaxies such as Hubble type and luminosity (Garnett & Shields 1987; Pagel 1991; Vila-Costas & Edmunds 1992; Dutil & Roy 1999). The oxygen abundance in the interstellar gas is usually used as a tracer of metallicity in late-type (spiral and irregular) galaxies at the current epoch. The study of abundance gradients in the discs of spiral galaxies was started by Searle (1971), with the recognition of a radial abundance gradient in M33. Results of investigations of variations in the gas composition within galaxies combined with results on the evolution of stellar populations provided the development of chemical evolution models (Chiappini, Romano & Matteucci 2003; Marcon-Uchida, Matteucci & Costa 2010).

A study of abundances and their gradients is based on measurements of emission-line spectra of individual H II regions in nearby galaxies. To define the parameters of the radial distributions of oxygen and nitrogen abundances (the extrapolated central intercept value and the gradient), the abundance measurements for a sufficiently large number of H II regions evenly distributed across the

⋆E-mail: gusev@sai.msu.ru

Table 1. The galaxy sample.

Galaxy	Type	B_t (mag)	RA[a] (J2000.0)	Dec.[a] (J2000.0)	Inclination (degree)	PA (degree)	v^b (km s^{-1})	R^c_{25} (arcmin)	R^c_{25} (kpc)	d (Mpc)	M_B (mag)
1	2	3	4	5	6	7	8	9	10	11	12
NGC 628	Sc	9.70	01 36 41.81	+15 47 00.3	7	25	659	5.23	10.96	7.2	−20.72
NGC 783	Sc	13.18	02 01 06.59	+31 52 56.2	43	57	5192	0.71	14.56	70.5	−22.01
NGC 2336	SB(R)bc	11.19	07 27 03.98	+80 10 41.1	55	175	2202	2.51	23.51	32.2	−22.14
NGC 6217	SB(R)bc	11.89	16 32 39.28	+78 11 53.6	33	162	1368	1.15	6.89	20.6	−20.45
NGC 7331	Sbc	10.20	22 37 04.16	+34 24 56.0	75	169	818	4.89	20.06	14.1	−21.68
NGC 7678	SBc	12.50	23 28 27.87	+22 25 14.0	44	21	3488	1.04	14.46	47.8	−21.55

[a]Coordinates of the galaxy centre. Units of right ascension are hours, minutes and seconds, and units of declination are degrees, arcminutes and arcseconds.
[b]Heliocentric radial velocity.
[c]Isophotal radius (25 mag arcsec^{-2} in the B band) corrected for Galactic extinction and absorption due to the inclination of a galaxy.

galaxy disc are necessary. Measurements of this kind are available for a limited number (∼50) of nearby galaxies (see compilations in Garnett 2002; Pilyugin, Vílchez & Contini 2004; Moustakas et al. 2010).

Here we report spectra of 63 H II regions in a sample of six spiral galaxies: NGC 628, NGC 783, NGC 2336, NGC 6217, NGC 7331 and NGC 7678. A first motivation of the spectral observations is determination of the oxygen and nitrogen abundances and electron temperatures in individual H II regions using the recent NS and ON calibrations (Pilyugin, Vílchez & Thuan 2010; Pilyugin & Mattsson 2011). The abundances will be used in the computation of the grid of evolutionary models of star clusters embedded in the H II regions studied. The second motivation is determination of the optical extinction by dust for the gas, from the measured Balmer decrement in the H II regions studied.

In this paper we describe the observations and data reduction, the derivation of elemental abundances, electron temperatures and optical extinction for individual H II regions and the examination their radial gradients across the discs. The results of these examinations provide information about the chemical abundance of the interstellar medium from which embedded stars formed, as well as the dust extinction estimations in the surrounding gas.

This paper is organized as follows. The observations and data reduction are described in Section 2. The oxygen and nitrogen abundances and the electron temperatures for individual H II regions as well the parameters of the radial distributions (the extrapolated central intercept value and the gradient) of the oxygen and nitrogen abundances and electron temperature in galaxies are discussed in Section 3. Section 4 gives a brief summary.

Throughout the paper, we will use the following notations for the line fluxes:

$$R_2 = [\mathrm{O\,II}]\lambda3727 + \lambda3729 = I_{[\mathrm{OII}]\lambda3727+\lambda3729}/I_{\mathrm{H}\beta}, \quad (1)$$

$$N_2 = [\mathrm{N\,II}]\lambda6548 + \lambda6584 = I_{[\mathrm{N\,II}]\lambda6548+\lambda6584}/I_{\mathrm{H}\beta}, \quad (2)$$

$$S_2 = [\mathrm{S\,II}]\lambda6717 + \lambda6731 = I_{[\mathrm{S\,II}]\lambda6717+\lambda6731}/I_{\mathrm{H}\beta}, \quad (3)$$

$$R_3 = [\mathrm{O\,III}]\lambda4959 + \lambda5007 = I_{[\mathrm{O\,III}]\lambda4959+\lambda5007}/I_{\mathrm{H}\beta}. \quad (4)$$

The electron temperatures t are given in units of 10^4 K.

2 OBSERVATIONS AND REDUCTION

We selected galaxies with known *UBVRI* photometry of H II regions, as obtained by our team in previous works: NGC 628 (Bruevich et al. 2007), NGC 783 (Gusev 2006a,b), NGC 2336 (Gusev & Park 2003), NGC 6217 (Artamonov et al. 1999), NGC 7331 (unpublished) and NGC 7678 (Artamonov, Bruevich & Gusev 1997). The galaxy sample is presented in Table 1. The columns show parameters from the LEDA data base (Paturel at al. 2003): morphological type and apparent magnitude of the galaxy in columns (2) and (3), coordinates (epoch 2000) in columns (4) and (5), the inclination and position angles in columns (6) and (7), radial velocity in column (8), the isophotal radius in arcmin and kpc in columns (9) and (10), distance in column (11) and absolute blue magnitude M_B in column (12).

2.1 Observations

The observations were carried out at the 6-m telescope of the Special Astrophysical Observatory (SAO) of the Russian Academy of Sciences with a spectral camera attached at the focal reducer SCORPIO (Afanasiev & Moiseev 2005) ($f/4 \rightarrow f/2.6$) in the multislit mode; the field was about 6 arcmin and the pixel size was 0.178 arcsec on n EEV 42–40 (2048 × 2048 pixels) CCD detector. The data for six galaxies were acquired during observing runs in 2006–2008 (see the journal of observations in Table 2).

The SCORPIO multislit unit is an arrangement that consists of 16 metal strips with slits located in the focal plane and moved in a 2.9 × 5.9 arcmin^2 field (Fig. 1). The size of the slits is 1.5 × 18 arcsec^2 while the distance between the centres of neighbouring slits is 22 arcsec.

Table 2. Journal of observations.

Object (Pos.[a])	Date	Exposures (s)	Seeing (arcsec)	Airmass
NGC 628 (1)	2008.02.07	900 × 2	1.9	2.03
NGC 783 (1)	2006.10.19	900 × 3	3.0	1.28
NGC 783 (2)	2007.09.07	900 × 4	1.6	1.02
NGC 783 (3)	2008.02.09	900 × 6	1.9	1.29
NGC 2336 (1)	2006.10.19	900 × 4	2.0	1.39
NGC 2336 (2)	2008.02.08	900 × 8	1.4	1.31
NGC 2336 (3)	2006.10.19	300 + 900	2.0	1.32
NGC 2336 (4)	2008.02.09	900 × 6	1.2	1.33
NGC 6217 (1)	2006.08.23	900 × 4	1.8	1.47
NGC 7331 (1)	2006.08.23	900 × 4	2.1	1.17
NGC 7678 (1)	2006.08.22	900 × 3	1.4	1.15
NGC 7678 (2)	2006.10.19	900 × 2	1.6	1.08
NGC 7678 (3)	2006.10.19	900 × 3	1.6	1.08

[a]Slit position.

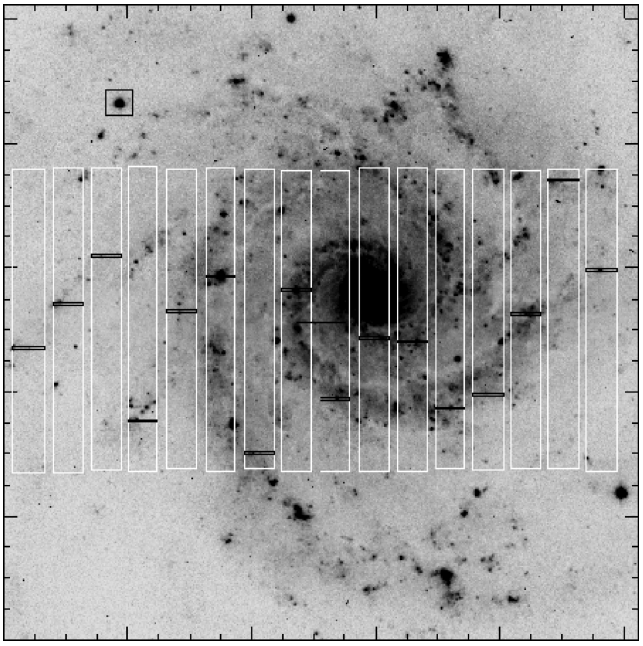

Figure 1. Disposition of 16 slits (black small horizontal rectangles) for NGC 628. North is upward and east is to the left ($PA_{slits} = 90^\circ$). The size of the image is 6.1×6.1 arcmin^2. The black square shows a guide star for the exposures.

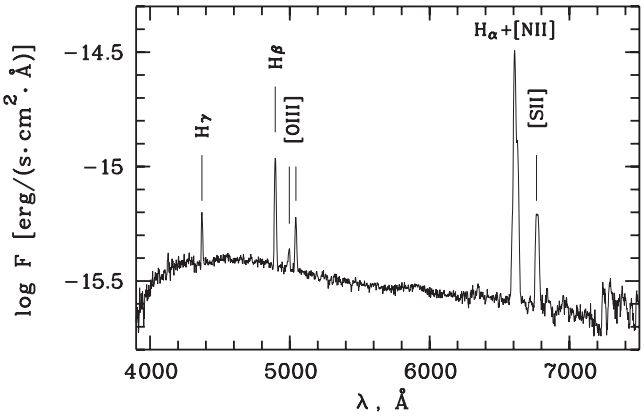

Figure 2. The observed spectrum 'b' of the H II region 17 in NGC 2336.

We used the grism VPHG550G with a dispersion of 2.1 Å pixel^{-1} and a spectral resolution of 10 Å, which provided spectral coverage from the [O II]λ3727+λ3729 oxygen emission lines to the [S II]λ6717+λ6731 sulphur emission lines. An example spectrum is presented in Fig. 2.

We selected target H II regions using *B*-band and Hα CCD images of galaxies, which were obtained with the 1-m and 1.5-m telescopes of the Mt Maidanak Observatory (Institute of Astronomy, Uzbek Academy of Sciences) in Uzbekistan and with the 1.8-m telescope of the Bohyunsan Optical Astronomy Observatory (Korea Astronomy and Space Science Institute) in Korea.

As mentioned above, the broad-band *UBVRI* photometry of selected H II regions, derived previously by us and our colleagues as part of our study of star-formation processes in spiral and irregular galaxies, provided a source of targets for multislit observations. We selected objects widely distributed across the face of the galaxies, enabling study of the chemical abundance gradients. The H II regions were selected for spectroscopy based on their brightness and size, with typical angular diameters from 2 up to 5 arcsec.

The total exposure time of the set consists of several time intervals. After every time interval, the positions of slits were displaced along the *X* axis with a step of 20 pixels. The *X* axis runs along the slit and the *Y* axis runs perpendicularly to the slit (see Fig. 1). This technique allows us to obtain spectra of several neighbouring H II regions using the same slit. Therefore, the exposure time for individual H II regions was smaller than the total exposure time of the set indicated in Table 2.

The observing procedure consisted of obtaining bias, flat and wavelength calibration images at the beginning and end of each set. Several spectrophotometric standards were observed during each night at different air mass.

2.2 Data reduction

Initial data reduction followed routine procedures, including bias, cosmic-ray, flat-field and atmospheric extinction corrections and photometric calibration, intensity normalization to the intensity of the central (8th) slit, wavelength calibration with a standard He–Ne–Ar lamp, subtracting the background, transformation to a one-dimensional spectrum and summing of spectra, using the European Southern Observatory Munich Image Data Analysis System (MIDAS).

The emission-line fluxes were measured using the continuum-substracted spectrum. Flux calibration was performed using standard stars BD+25°4655, HZ2, HZ4, Feige 34 and G193–74 (Oke 1990). Both the spectra of standard stars and the SAO astroclimate data of Kartasheva & Chunakova (1978) were used for a calculation of the extinction coefficient and a correction for atmospheric extinction. The blended lines Hα+[N II]λ6548+λ6584 and [S II]λ6717+λ6731 were measured by three or two-Gaussian fitting, respectively.

The extraction aperture corresponded to the area where the brightest emission lines from H II regions were 'visible' above the noise. This size is close to the angular diameter of individual H II regions from the imaging surveys as projected along the PA of the slit.

Coordinates, deprojected galactocentric distances and radial velocities are listed in Table 3. Reddening-corrected line intensities $I(\lambda)/I(\mathrm{H}\beta)$, undereddened fluxes $F(\mathrm{H}\beta)$ and the logarithmic extinction coefficients $c(\mathrm{H}\beta)$ are given in Table 4. Though the sulphur lines [S II]λ6717 and [S II]λ6731 were deblended in several cases, the accuracy was very low. Therefore Table 4 presents the sum of [S II](λ6717+λ6731) of sulphur lines. Some H II regions were observed twice; they are marked with letters 'a' and 'b' in Tables 3 and 4.

Absolute emission-line fluxes derived for the same object on different nights can differ for the following reasons: (i) different seeing on different nights and (ii) a slight deviation of the slit from the previous position. Note that the apparent sizes of the studied H II regions are generally larger than the width of the slit. It should be noted that, although the absolute emission-line fluxes can differ by a large amount between different observations depending on the exact slit placement, flux ratios derived for the same object on different nights coincide within the errors (see Table 4).

During calculation of the error in the line-intensity measurement, the following factors have been taken into consideration. The first factor is related to the Poisson statistics of the line photon flux. The second factor of the error appears in the computation of the underlying continuum, and makes the main contribution to the inaccuracy of faint lines. The third factor concerns the uncertainty

Table 3. Offsets, galactocentric distances, radial velocities of H II regions.

H II region	Pos.[a]	Ref.[b]	N–S[c] (arcsec)	E–W[c] (arcsec)	r^d (kpc)	v^e (km s^{-1})
			NGC 628			
1	1	94, 54	+12.5	+129.0	4.55	620
2	1	92	−12.0	+87.7	3.11	665
3	1	77, 58	−64.3	+36.5	2.58	611
4	1	75	−65.4	+45.0	2.77	638
5	1	73, 11	−28.8	+25.3	1.34	654
6	1	25, 6	+0.2	−43.0	1.51	655
7	1	62, 81	−91.8	−68.1	4.01	628
8	1	58	−72.0	−132.6	5.31	614
9	1	35	+19.7	−153.1	5.42	716
10	1	38, (5)	−6.4	−177.9	6.25	711
			NGC 783			
1	1	–	−24.3	+16.0	10.60	5181
2	1	–	−27.5	+23.7	12.83	5202
3	1	–	−4.8	−19.7	8.33	5192
4	1	–	+19.5	−29.1	11.96	5235
5	2	–	−19.5	+22.1	10.17	5270
6	2	–	−20.0	+25.6	11.15	5103
7	2	–	+21.6	−28.3	12.20	5153
8	3	–	+5.1	−22.9	8.42	5233
			NGC 2336			
1a	1	–	−113.8	+33.5	20.79	2011
1b	2	–	−113.8	+33.5	20.79	2048
2	1	28	−89.0	−40.0	16.89	2006
3	1	27a	−71.8	+0.2	11.30	2040
4a	1	26	−47.8	−10.5	7.79	2009
4b	4	26	−47.8	−10.5	7.79	2052
5	1	22	−27.5	−9.8	4.86	2028
6	1	17	+17.5	+85.4	23.02	2264
7a	1	5	+95.9	+13.6	15.19	2432
7b	2	5	+95.9	+13.6	15.19	2410
8	2	27d	−82.5	−9.5	12.99	2013
9	2	–	−62.6	+8.1	10.27	1917
10a	2	19	+3.4	+43.8	11.82	2141
10b	4	19	+3.4	+43.8	11.82	2198
11	2	16	+18.2	+38.7	10.59	2349
12	2	10	+52.3	+0.2	8.22	2512
13	2	8	+68.1	−34.5	14.84	2485
14a	2	2	+142.0	−11.5	22.83	2573
14b	4	2	+142.0	−11.5	22.83	2545
15a	3	30	−109.0	−32.1	18.49	1940
15b	4	30	−109.0	−32.1	18.49	1935
16a	3	27b	−77.3	−3.6	12.11	2014
16b	4	27b	−77.3	−3.6	12.11	2018
17a	3	21	−26.1	+48.3	14.05	2167
17b	4	21	−26.1	+48.3	14.05	2061
18	4	29	−94.5	−37.3	17.18	2233
19	4	27e	−83.9	−4.3	13.13	2064
20	4	–	−31.6	+48.6	14.49	2160
21	4	–	−19.3	+47.6	13.50	1982
22	4	–	+27.2	−62.7	17.88	2364
23	4	15	+24.4	−61.7	17.47	2263
24	4	9	+62.6	+48.3	15.61	2375
25	4	–	+67.7	+44.5	15.32	2443
26	4	–	+77.7	−5.3	12.43	2575
27	4	7	+80.8	−4.6	12.88	2422
28	4	4	+111.7	−31.1	20.17	2335
			NGC 6217			
1	1	–	+29.8	+13.9	3.30	1443
2	1	–	+42.2	+13.0	4.41	1485
3	1	–	−14.6	+23.2	3.24	1348
			NGC 7331			
1	1	–	+123.2	+40.4	9.78	537
2	1	–	+76.8	+18.0	5.45	512
3	1	–	+27.4	+16.2	3.48	667
4	1	1	−50.2	+23.1	9.06	865
			NGC 7678			
1	1	–	−54.2	+12.6	13.02	3422
2	1	–	−31.8	−7.1	8.57	3431
3	1	–	−23.3	−14.8	8.10	3525
4	1	–	−14.5	−21.0	8.11	3553
5	1	–	+3.7	−26.6	8.15	3455
6	2	–	−26.5	+14.2	7.02	3412
7	2	–	−10.5	+31.6	9.63	3415
8a	2	–	−15.8	+27.3	8.56	3426
8b	3	–	−15.8	+27.3	8.56	3432
9	3	–	−46.5	−5.2	11.87	3384
10	3	–	−23.0	+6.2	5.56	3398

[a]Slit position.
[b]H II region number from Belley & Roy (1992) (first number), Rosales-Ortega et al. (2011) (second number) and van Zee et al. (1998) (second number in brackets) for NGC 628, from Gusev & Park (2003) for NGC 2336 and from Bresolin, Kennicutt & Garnett (1999) for NGC 7331.
[c]Offsets from the Galactic Centre (see Table 1), positive to the north and west.
[d]Deprojected galactocentric distance.
[e]Radial velocity of H II region (km s^{-1}).

of the spectral sensitivity curve. It gives an additional error to the relative line intensities. The last factor is related to the goodness of fit of the line profile and is crucial for blended lines. All these components are summed in quadrature. The total errors have been propagated to calculate the errors of all derived parameters.

Estimations of radial velocities of the studied H II regions (last column in Table 3) were derived as a by-product through the measurements of Doppler shifts of the Hα line in spectra. The accuracy of radial velocity measurements is about 30 km s^{-1}. Analysis of the observed radial velocities is beyond the scope of this paper.

The measured emission fluxes F were corrected for interstellar reddening and Balmer absorption in the underlying stellar continuum. We used the theoretical Hα to Hβ ratio from Osterbrock (1989), assuming case B recombination and an electron temperature of 10 000 K and the analytical approximation to the Whitford interstellar reddening law by Izotov, Thuan & Lipovetsky (1994). We adopted the absorption equivalent width $\mathrm{EW_a}(\lambda) = 2$ Å for hydrogen lines for all objects, which is the mean value for H II regions derived by McCall, Rybski & Shields (1985). For lines other than hydrogen, $\mathrm{EW_a}(\lambda) = 0$. The uncertainty in the logarithmic extinction coefficient $c(\mathrm{H}\beta)$ is calculated from the measurement errors of Hα and Hβ lines and propagated to the dereddened line ratios.

2.3 Comparison with previous observations

H II regions in the galaxies NGC 628 and NGC 7331 have previously been observed via spectroscopy (McCall et al. 1985; Ferguson, Gallagher & Wyse 1998; van Zee et al. 1998; Bresolin, Kennicutt & Garnett 1999) or spectrophotometric imaging (Belley & Roy 1992) or the integral field spectroscopy method (Rosales-Ortega et al. 2011). There is only one overlap with previous spectroscopic

Table 4. The reddening-corrected fluxes of the main emission lines of H II regions.

H II region	[O II][a] 3727+3729	[O III][a] 5007	[N II][a] 6584	[S II][a] 6717+6731	$F(H\beta)$[b] 4861	$c(H\beta)$
			NGC 628			
1	–	–	0.73 ± 0.41	0.42 ± 0.24	7.48 ± 1.17	0.74 ± 0.31
2	–	–	1.06 ± 0.42	1.16 ± 0.45	8.04 ± 0.85	0.58 ± 0.24
3	–	–	0.61 ± 0.26	0.35 ± 0.14	27.40 ± 3.07	0.33 ± 0.21
4	–	0.31 ± 0.13	0.46 ± 0.35	0.54 ± 0.30	5.21 ± 0.79	0.37 ± 0.31
5	–	–	0.70 ± 0.35	0.78 ± 0.35	9.61 ± 1.08	0.30 ± 0.25
6	–	–	–	–	2.12 ± 0.80	0.85 ± 0.96
7	5.64 ± 2.01	0.49 ± 0.07	0.79 ± 0.22	0.47 ± 0.12	33.32 ± 1.82	0.00 ± 0.13
8	4.06 ± 1.74	0.66 ± 0.07	0.77 ± 0.18	0.51 ± 0.10	38.15 ± 2.05	0.12 ± 0.12
9	–	1.62 ± 0.18	0.59 ± 0.16	0.32 ± 0.08	22.62 ± 1.41	0.87 ± 0.13
10	–	0.36 ± 0.10	0.74 ± 0.29	0.77 ± 0.30	30.51 ± 3.80	0.03 ± 0.22
			NGC 783			
1	–	1.47 ± 0.20	1.06 ± 0.27	0.72 ± 0.20	5.81 ± 0.38	0.28 ± 0.15
2	–	0.73 ± 0.30	–	–	1.38 ± 0.36	0.08 ± 0.55
3	1.80 ± 0.60	0.23 ± 0.04	1.33 ± 0.20	0.89 ± 0.13	22.15 ± 6.51	0.51 ± 0.09
4	–	0.68 ± 0.13	1.46 ± 0.46	1.19 ± 0.39	3.34 ± 0.29	0.90 ± 0.20
5	2.34 ± 0.68	0.23 ± 0.04	0.54 ± 0.14	0.86 ± 0.15	7.78 ± 0.31	0.61 ± 0.10
6	2.45 ± 0.53	0.44 ± 0.05	1.50 ± 0.21	1.16 ± 0.17	11.69 ± 0.42	0.44 ± 0.09
7	–	1.25 ± 0.46	3.11 ± 1.87	2.30 ± 1.46	2.55 ± 0.46	0.76 ± 0.45
8	2.35 ± 0.54	0.32 ± 0.06	1.16 ± 0.19	0.64 ± 0.12	25.97 ± 1.00	0.73 ± 0.09
			NGC 2336			
1a	–	0.61 ± 0.23	1.15 ± 0.59	1.05 ± 0.53	2.04 ± 0.35	0.46 ± 0.33
1b	4.16 ± 1.07	1.01 ± 0.11	0.89 ± 0.18	1.37 ± 0.24	6.80 ± 0.33	0.15 ± 0.11
2	2.26 ± 0.66	0.58 ± 0.05	0.81 ± 0.12	0.51 ± 0.07	22.07 ± 0.77	0.45 ± 0.08
3	–	0.27 ± 0.07	0.80 ± 0.23	0.44 ± 0.14	16.36 ± 1.18	0.69 ± 0.16
4a	–	–	0.66 ± 0.16	0.47 ± 0.10	7.83 ± 0.40	0.71 ± 0.12
4b	–	–	0.82 ± 0.22	0.57 ± 0.15	22.58 ± 1.29	0.34 ± 0.14
5	–	–	0.91 ± 0.56	–	2.70 ± 0.31	0.34 ± 0.32
6	–	1.42 ± 0.06	0.48 ± 0.08	0.62 ± 0.07	19.92 ± 0.53	1.12 ± 0.06
7a	–	0.48 ± 0.09	0.85 ± 0.23	0.66 ± 0.19	5.37 ± 0.38	0.46 ± 0.15
7b	–	0.27 ± 0.02	0.88 ± 0.11	0.66 ± 0.08	35.97 ± 0.98	0.45 ± 0.06
8	2.21 ± 0.48	0.14 ± 0.02	0.71 ± 0.11	0.66 ± 0.08	28.12 ± 0.70	0.32 ± 0.07
9	–	0.05 ± 0.01	0.77 ± 0.13	0.60 ± 0.09	20.06 ± 0.56	0.11 ± 0.08
10a	–	0.16 ± 0.03	1.07 ± 0.17	0.80 ± 0.13	18.14 ± 0.63	0.46 ± 0.09
10b	–	0.17 ± 0.02	1.01 ± 0.13	0.70 ± 0.08	33.81 ± 0.96	0.64 ± 0.07
11	–	0.47 ± 0.08	1.17 ± 0.27	1.14 ± 0.26	8.42 ± 0.55	0.90 ± 0.14
12	–	–	0.85 ± 0.36	0.79 ± 0.34	4.94 ± 0.62	0.93 ± 0.26
13	–	0.35 ± 0.04	1.04 ± 0.15	0.60 ± 0.09	11.16 ± 0.38	1.23 ± 0.08
14a	–	1.15 ± 0.10	0.91 ± 0.16	0.98 ± 0.16	18.31 ± 0.82	0.72 ± 0.10
14b	3.36 ± 0.76	1.18 ± 0.07	0.79 ± 0.11	0.87 ± 0.10	20.25 ± 0.66	0.70 ± 0.07
15a	–	1.68 ± 0.54	0.65 ± 0.51	–	2.47 ± 0.44	0.21 ± 0.40
15b	6.36 ± 2.07	0.89 ± 0.11	0.66 ± 0.18	0.78 ± 0.20	9.32 ± 0.47	0.07 ± 0.13
16a	2.07 ± 0.92	0.32 ± 0.08	0.73 ± 0.20	0.79 ± 0.20	9.31 ± 0.65	0.66 ± 0.15
16b	2.63 ± 0.61	0.21 ± 0.03	0.73 ± 0.12	0.68 ± 0.09	26.12 ± 0.75	0.56 ± 0.07
17a	–	0.25 ± 0.06	0.92 ± 0.25	0.73 ± 0.20	15.98 ± 1.32	0.38 ± 0.16
17b	–	0.32 ± 0.02	1.22 ± 0.11	0.65 ± 0.05	99.43 ± 1.82	0.62 ± 0.05
18	–	–	0.75 ± 0.47	0.89 ± 0.56	3.63 ± 0.66	1.32 ± 0.38
19	7.54 ± 2.31	0.23 ± 0.07	0.72 ± 0.20	0.82 ± 0.20	13.78 ± 0.88	0.71 ± 0.14
20	–	0.24 ± 0.08	1.11 ± 0.25	0.89 ± 0.21	8.53 ± 0.57	1.06 ± 0.13
21	–	0.30 ± 0.05	1.73 ± 0.31	0.94 ± 0.20	8.93 ± 0.43	0.35 ± 0.12
22	1.78 ± 0.29	0.53 ± 0.02	0.81 ± 0.08	0.60 ± 0.05	22.86 ± 0.44	0.49 ± 0.05
23	1.88 ± 0.25	0.68 ± 0.02	0.85 ± 0.08	0.60 ± 0.04	42.42 ± 0.74	0.09 ± 0.04
24	–	0.76 ± 0.20	1.33 ± 0.52	1.24 ± 0.52	3.62 ± 0.42	0.84 ± 0.25
25	–	0.82 ± 0.16	0.87 ± 0.25	0.71 ± 0.22	5.12 ± 0.41	0.86 ± 0.17
26	–	0.47 ± 0.22	1.34 ± 0.64	1.13 ± 0.55	5.96 ± 0.93	0.92 ± 0.32
27	–	0.72 ± 0.22	1.39 ± 0.56	1.21 ± 0.54	4.56 ± 0.44	0.50 ± 0.25
28	2.37 ± 0.40	0.70 ± 0.03	0.89 ± 0.09	0.69 ± 0.08	38.60 ± 0.81	0.08 ± 0.05
			NGC 6217			
1	1.87 ± 0.81	0.25 ± 0.05	0.85 ± 0.16	0.52 ± 0.10	21.24 ± 0.86	0.10 ± 0.10
2	–	–	1.09 ± 0.52	0.89 ± 0.42	7.37 ± 1.14	0.76 ± 0.31

Table 4 – *continued*

H II region	[O II]^a 3727+3729	[O III]^a 5007	[N II]^a 6584	[S II]^a 6717+6731	$F(H\beta)^b$ 4861	$c(H\beta)$
			NGC 6217			
3	–	0.98 ± 0.31	1.08 ± 0.43	0.71 ± 0.29	7.70 ± 1.03	0.80 ± 0.25
			NGC 7331			
1	–	1.05 ± 0.22	1.20 ± 0.57	0.91 ± 0.44	3.16 ± 0.36	0.09 ± 0.28
2	–	–	2.65 ± 2.33	0.91 ± 0.90	1.13 ± 0.31	1.53 ± 0.68
3	–	0.14 ± 0.06	0.44 ± 0.16	0.26 ± 0.09	9.27 ± 0.79	1.24 ± 0.17
4	2.32 ± 1.15	0.41 ± 0.04	0.99 ± 0.14	0.82 ± 0.10	26.64 ± 0.88	0.50 ± 0.08
			NGC 7678			
1	–	1.17 ± 0.58	0.82 ± 0.68	0.88 ± 0.71	3.03 ± 0.81	0.94 ± 0.51
2	–	0.52 ± 0.14	1.01 ± 0.36	0.83 ± 0.29	6.34 ± 0.59	0.32 ± 0.21
3	2.74 ± 0.91	0.30 ± 0.05	0.48 ± 0.13	0.67 ± 0.14	28.74 ± 1.30	0.14 ± 0.10
4	2.00 ± 0.54	0.49 ± 0.05	0.74 ± 0.13	0.60 ± 0.10	29.05 ± 1.10	0.30 ± 0.08
5	4.07 ± 1.78	0.39 ± 0.12	1.47 ± 0.42	0.77 ± 0.27	7.57 ± 0.60	0.06 ± 0.19
6	–	0.31 ± 0.08	1.05 ± 0.24	0.97 ± 0.21	9.54 ± 0.61	0.77 ± 0.14
7	–	0.63 ± 0.03	0.89 ± 0.09	0.85 ± 0.06	61.66 ± 1.21	0.69 ± 0.05
8a	–	0.54 ± 0.02	0.85 ± 0.08	0.69 ± 0.04	196.70 ± 3.16	0.80 ± 0.04
8b	–	0.50 ± 0.02	0.91 ± 0.08	0.62 ± 0.04	101.40 ± 1.63	0.90 ± 0.04
9	–	0.67 ± 0.04	1.04 ± 0.13	0.63 ± 0.08	17.35 ± 0.52	0.79 ± 0.07
10	2.53 ± 0.44	0.44 ± 0.02	0.95 ± 0.10	0.93 ± 0.08	41.05 ± 0.81	0.71 ± 0.05

$^a I(\lambda)/I(H\beta)$ ratio.
^{b}The fluxes are in units of 10^{-16} erg s^{-1} cm^{-2}.

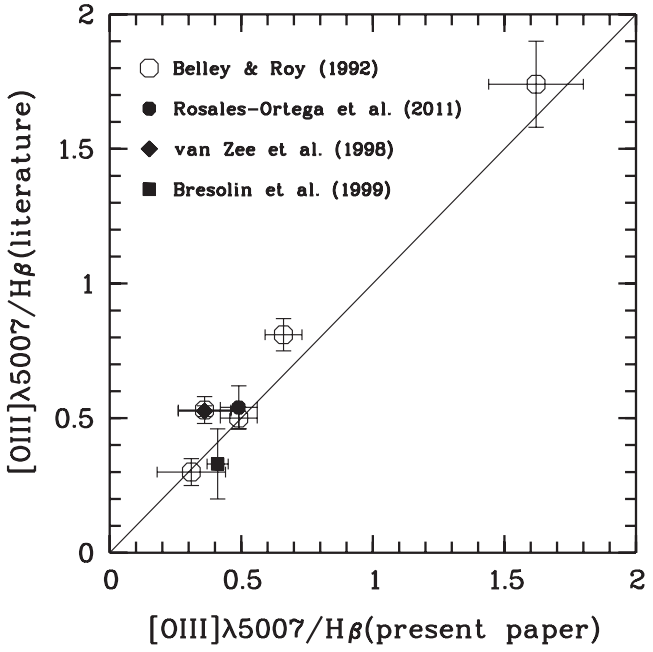

Figure 3. Comparison between redding-corrected fluxes [O III]λ5007/Hβ obtained in the present paper and data from the literature (Belley & Roy 1992; van Zee et al. 1998; Bresolin et al. 1999; Rosales-Ortega et al. 2011) for common H II regions.

observations in each galaxy: one object in NGC 628 observed by van Zee et al. (1998) and one object in NGC 7331 observed by Bresolin et al. (1999). In Fig. 3 we compared our measurements with the results of these two previous spectroscopic observations, the results of the spectrophotometric imaging (Belley & Roy 1992), which are not as accurate as spectroscopic ones for individual objects, and the results of integral field spectroscopy for NGC 628 (one object (Rosales-Ortega et al. 2011); see Table 3).

Fig. 3 shows a satisfactory agreement between our spectroscopy and previous observations. Note that for the quantitative analysis more statistics information is necessary. Previous spectroscopic observations of H II regions in NGC 628 and NGC 7331 will be also compared in Section 3 via radial oxygen and nitrogen abundance distributions in the discs of parent galaxies.

3 ABUNDANCES

Here we use the spectral data presented in Section 2 for determination of the oxygen and nitrogen abundances (and electron temperatures) in H II regions, aiming to establish the radial distributions of these elements across the discs of galaxies.

3.1 Preliminary remarks

Since our measurements of the [N II]λ6584 and [O III]λ5007 lines are more reliable than those of the [N II]λ6548 and [O III]λ4959 lines, we used [N II]λ6584 and [O III]λ5007 lines only. The [O III]λ5007 and λ4959 lines originate from transitions from the same energy level, so their flux ratio is due only to the transition probability ratio, which is 3.013 (Storey & Zeippen 2000). Hence, the value of R_3 can be well approximated by

$$R_3 = 1.33\ I_{[\mathrm{O\,III}]\lambda5007}/I_{\mathrm{H}\beta}. \quad (5)$$

Similarly, the [N II]λ6584 and λ6548 lines also originate from transitions from the same energy level and the transition probability ratio for those lines is 3.071 (Storey & Zeippen 2000). The value of N_2 is therefore well approximated by

$$N_2 = 1.33\ I_{[\mathrm{N\,II}]\lambda6584}/I_{\mathrm{H}\beta}. \quad (6)$$

We have used equation (6) instead of equation (2) to obtain the value of N_2 and equation (5) instead of equation (4) to determine the value of R_3.

The intensities of strong, easily measured lines can be used to separate different types of emission-line objects according to their main excitation mechanism. Baldwin, Phillips & Terlevich (1981) proposed a diagram (BPT classification diagram) where

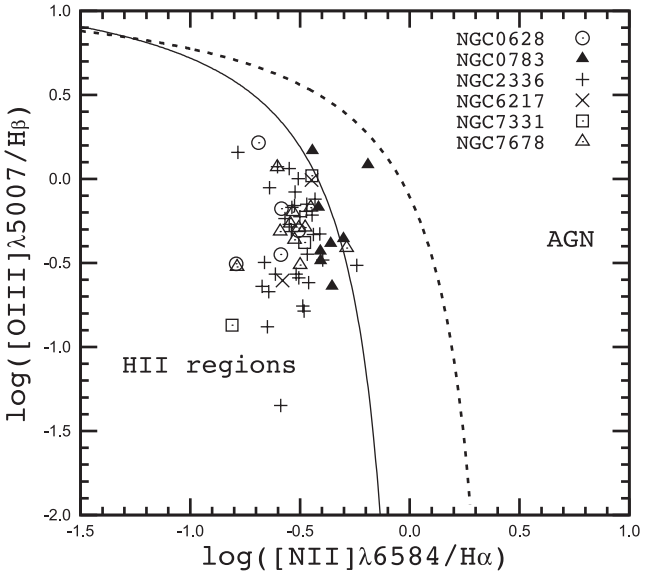

Figure 4. The [N II]λ6584/Hα versus [O III]λ5007/Hβ diagram. The symbols are the H II regions. The solid line separates objects with H II spectra from those containing an AGN according to Kauffmann et al. (2003). The dashed line is the separation line from Kewley et al. (2001).

the excitation properties of H II regions are studied by plotting the low-excitation [N II]λ6584/Hα line ratio against the high-excitation [O III]λ5007/Hβ line ratio.

The [N II]λ6584/Hα versus [O III]λ5007/Hβ diagram is shown in Fig. 4. The symbols are H II regions. The solid line represents the relation

$$\log([\mathrm{O\,III}]\lambda5007/\mathrm{H}\beta) = \frac{0.61}{\log([\mathrm{N\,II}]\lambda6584/\mathrm{H}\alpha) - 0.05} + 1.3, \quad (7)$$

which separates objects with H II spectra from those containing an active galactic nucleus (AGN) (Kauffmann et al. 2003). The dashed separation line is the relation

$$\log([\mathrm{O\,III}]\lambda5007/\mathrm{H}\beta) = \frac{0.61}{\log([\mathrm{N\,II}]\lambda6584/\mathrm{H}\alpha) - 0.47} + 1.19 \quad (8)$$

from Kewley et al. (2001). Fig. 4 shows that all H II regions from our sample are thermally photoionized objects if the separation line from Kewley et al. (2001) is used. When the separation line from Kauffmann et al. (2003) is used then one object (No. 7 in NGC 783) has an appreciable shift from the separation line towards the AGNs. However, the uncertainty in the measurement of the intensity of the [N II]λ6584 line is large for this object (see Table 4). Therefore all H II regions are included for further consideration. The abundances determined for object No. 7 from NGC 783 are not considered to be in question.

3.2 Abundances and temperatures

Accurate oxygen and nitrogen abundances in H II regions can be derived via the classic T_e method, often referred to as the direct method. This method is based on the measurement of the electron temperature t_3 within the [O III] zone and/or the electron temperature t_2 within the [O II] zone. The ratio of the nebular to auroral oxygen line intensities [O III](λ4959+λ5007)/[O III]λ4363 is usually used for the t_3 determination, while the ratios of the nebular to auroral nitrogen line intensities [N II](λ6548 + λ6584)/[N II]λ5755 or [O II](λ3727 + λ3729)/[O II](λ7320 + λ7330) are used for the t_2 determination. The auroral lines in spectra of H II regions from our sample are too faint to be detected. In this case, it is still possible to obtain the estimates of the nebular abundances, using intensity ratios of the brightest ionic emission lines.

Pagel et al. (1979) and Alloin et al. (1979) have suggested that the locations of H II regions in some emission-line diagrams can be calibrated in terms of their oxygen abundances. This approach to abundance determination in H II regions, usually referred to as the 'strong-line method' has been widely adopted, especially in cases where the temperature-sensitive auroral lines are not detected. Numerous relations have been proposed to convert metallicity-sensitive emission-line ratios into metallicity or temperature estimates (e.g. Dopita & Evans 1986; Zaritsky et al. 1994; Vilchez & Esteban 1996; Pilyugin 2000, 2001; Pettini & Pagel 2004; Tremonti et al. 2004; Pilyugin & Thuan 2005; Liang et al. 2006; Stasińska 2006; Thuan, Pilyugin & Zinchenko 2010; see the reviews in Ellison et al. 2008 and López-Sánchez & Esteban 2010 for more details).

Two calibration relations for estimation of the oxygen and nitrogen abundances of H II regions have recently been suggested. The ON calibration relations give the oxygen and nitrogen abundances and electron temperature in terms of fluxes of the strong emission lines O^{++}, O^{+} and N^{+} (Pilyugin et al. 2010). The NS calibration relations give abundances and electron temperatures in terms of fluxes in the strong emission lines of O^{++}, N^{+} and S^{+} (Pilyugin & Mattsson 2011). The ON and NS calibrations provide reliable oxygen and nitrogen abundances for H II regions of all metallicities. The oxygen R_2 line is measured in presented spectra with a large uncertainty (or sometimes even unavailable). Therefore we use the NS calibration method to estimate the abundances and electron temperatures in our sample of H II regions.

Both individual H II regions excited by a single source (single star or star cluster) and giant H II regions can be observed in nearby galaxies. Giant H II regions can be composite nebulae that contain a number of H II regions with different physical properties, all contributing to the global spectrum (Kennicutt 1984). The ON and NS calibrations give oxygen and nitrogen abundances in composite nebulae that agree with the mean luminosity-weighted abundances of their components to within ∼0.2 dex (Pilyugin et al. 2012).

The calibrations are constructed under the assumption that the H II regions are in the low-density regime. Since the sulphur lines [S II]λ6717 and [S II]λ6731 in most of our spectra are blended ([S II]λ6717 and [S II]λ6731 were deblended in several cases only and with low accuracy), we cannot estimate the density-sensitive ratio [S II]λ6717/[S II]λ6731 and verify the low-density regime in our objects. Therefore we assume that the H II regions of our sample are all in the low-density regime, which is typical for the majority of extragalactic H II regions (Zaritsky et al. 1994; Bresolin et al. 2005; Gutiérrez & Beckman 2010).

In previous works, little attention was paid to the radial distribution of nitrogen abundances in the discs of spiral galaxies, despite the fact that such studies would have several advantages (Thuan et al. 2010). First, since at $12 + \log(\mathrm{O/H}) \gtrsim 8.3$ secondary nitrogen becomes dominant and the nitrogen abundance increases at a faster rate than the oxygen abundance (Henry, Edmunds & Köppen (2000), the change in nitrogen abundances with galactocentric distance should show a larger amplitude in comparison with oxygen abundances and, as a consequence, the gradient (and differences in gradients among galaxies) should be easier to detect. Furthermore, there is a time delay in the nitrogen production compared with oxygen production (Maeder 1992; van den Hoek & Groenewegen 1997; Pagel 1997; Pilyugin & Thuan 2011). This provides an additional constraint on the chemical evolution of galaxies. For these reasons,

Table 5. Oxygen and nitrogen abundances and electron temperatures t_2 in H II regions derived using the NS calibrations.

H II region	R_G [a]	12+log(O/H)$_{NS}$	12+log(N/H)$_{NS}$	t$_{NS}$ [b]
		NGC 628		
4	0.25	8.36	7.16	0.77
7	0.37	8.58	7.79	0.74
8	0.48	8.55	7.70	0.77
9	0.49	8.56	7.57	0.82
10	0.57	8.56	7.64	0.75
		NGC 783		
1	0.73	8.42	7.57	0.88
3	0.57	8.56	7.90	0.71
4	0.82	8.46	7.65	0.81
6	0.77	8.46	7.74	0.79
7	0.84	8.34	7.61	0.91
8	0.58	8.57	7.91	0.72
		NGC 2336		
1a	0.88	8.47	7.61	0.81
1b	0.88	8.38	7.32	0.91
2	0.72	8.56	7.75	0.75
3	0.48	8.66	7.92	0.68
6	0.98	8.40	7.18	0.88
7a	0.65	8.54	7.69	0.76
7b	0.65	8.59	7.80	0.71
8	0.55	8.68	7.83	0.66
9	0.44	8.78	8.09	0.59
10a	0.50	8.63	7.90	0.68
10b	0.50	8.63	7.92	0.68
11	0.45	8.47	7.63	0.80
13	0.63	8.58	7.87	0.72
14a	0.97	8.43	7.43	0.88
14b	0.97	8.44	7.41	0.87
15b	0.79	8.47	7.43	0.84
16a	0.52	8.59	7.63	0.73
16b	0.52	8.64	7.76	0.69
17a	0.60	8.59	7.80	0.71
17b	0.60	8.57	7.92	0.72
19	0.56	8.62	7.66	0.71
20	0.62	8.57	7.81	0.72
21	0.57	8.52	7.94	0.74
22	0.76	8.54	7.69	0.76
23	0.74	8.52	7.68	0.78
24	0.66	8.44	7.57	0.84
25	0.65	8.48	7.59	0.82
26	0.53	8.50	7.69	0.78
27	0.55	8.47	7.61	0.81
28	0.86	8.50	7.64	0.79
		NGC 6217		
1	0.48	8.65	7.89	0.68
3	0.47	8.46	7.65	0.83
		NGC 7331		
1	0.49	8.44	7.59	0.85
3	0.17	8.41	7.39	0.69
4	0.45	8.53	7.71	0.76
		NGC 7678		
1	0.90	8.45	7.42	0.87
2	0.59	8.51	7.67	0.78
3	0.56	8.30	6.98	0.80
4	0.56	8.55	7.67	0.76
5	0.56	8.52	7.92	0.75
6	0.49	8.55	7.71	0.74
7	0.67	8.49	7.58	0.80
8a	0.59	8.53	7.66	0.77
8b	0.59	8.54	7.74	0.76
9	0.82	8.51	7.75	0.78
10	0.38	8.52	7.63	0.77

[a] In units of isophotal radius R_{25}.
[b] t_2 in units of 10^4 K.

not only the radial distribution of oxygen abundances but also that of nitrogen abundances is estimated here.

The resultant NS calibration abundances and electron temperatures are given in Table 5. The oxygen and nitrogen abundances and electron temperature were derived for H II regions where R_3, N_2, and S_2 lines are available. It should be noted that the NS calibration relations have been derived using the spectra of H II regions with well-measured electron temperatures as calibration data points. Therefore, the NS calibration relations produce abundances that are in agreement with the abundance scale defined by the classic T_e method.

The O/H–N/O diagram gives the possibility of testing the validity of the abundances determined. On the O/H–N/O diagram (Fig. 5) we compare abundances of 50 H II regions in six studied galaxies (see legend) with T_e-based abundances of the best-studied H II regions (open circles) in nearby galaxies (data compiled from Pilyugin et al. 2010). One can see from Fig. 5 that all points lie within the spread of Pilyugin et al. (2010), i.e. the abundances in our sample of H II regions derived using the NS calibration occupy the same band in the O/H–N/O diagram as the T_e-based abundances in the sample of best-studied H II regions in nearby galaxies. This shows that our abundance estimations based on the NS calibration method are realistic.

3.3 Radial abundance gradients

It is common practice (e.g. Zaritsky et al. 1994; van Zee et al. 1998; Pilyugin et al. 2004) that the radial oxygen abundance distribution in the disc of a spiral galaxy is fitted by an expression of the type

$$12 + \log(\mathrm{O/H}) = 12 + \log(\mathrm{O/H})_0 + C_{\mathrm{O/H}} \times (R/R_{25}), \qquad (9)$$

where $12 + \log(\mathrm{O/H})_0$ is the extrapolated central oxygen abundance, $C_{\mathrm{O/H}}$ is the slope of the oxygen abundance gradient expressed in terms of dex/R_{25} and R/R_{25} is the fractional radius (the

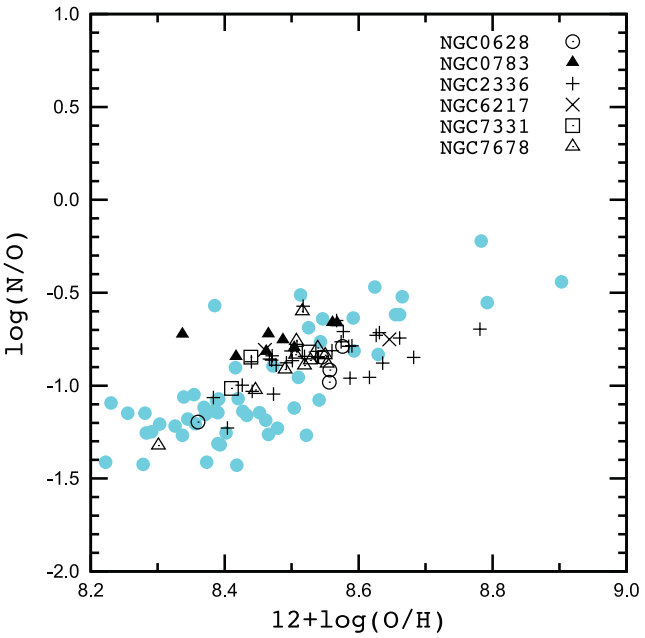

Figure 5. The O/H–N/O diagram. The different symbols marked in the legend show abundances derived using the NS calibration for our sample of H II regions. The filled circles show T_e-based abundances in the sample of best-studied H II regions in nearby galaxies (the compilation of data from Pilyugin et al. (2010)).

galactocentric distance normalized to the disc isophotal radius). Analogously to the case of oxygen abundance, the radial nitrogen abundance distribution in the disc of a spiral galaxy is fitted by an equation of the type

$$12 + \log(\mathrm{N/H}) = 12 + \log(\mathrm{N/H})_0 + C_{\mathrm{N/H}} \times (R/R_{25}). \quad (10)$$

Fig. 6 shows the radial oxygen (left column) and nitrogen (right column) abundance distributions in the discs of spiral galaxies NGC 628, NGC 783, NGC 2336, NGC 7331 and NGC 7678. The abundances derived from our spectral data are shown by filled circles.

The emission-line measurements in the spectra of H II regions in the disc of galaxy NGC 628 were previously reported by McCall et al. (1985), Ferguson et al. (1998), van Zee et al. (1998) and Bresolin et al. (1999) and those in the disc of galaxy NGC 7331 were given by McCall et al. (1985) and Ferguson et al. (1998).

As noted in Section 2.3, there are only two objects in NGC 628 and NGC 7331 in common with previous spectroscopic

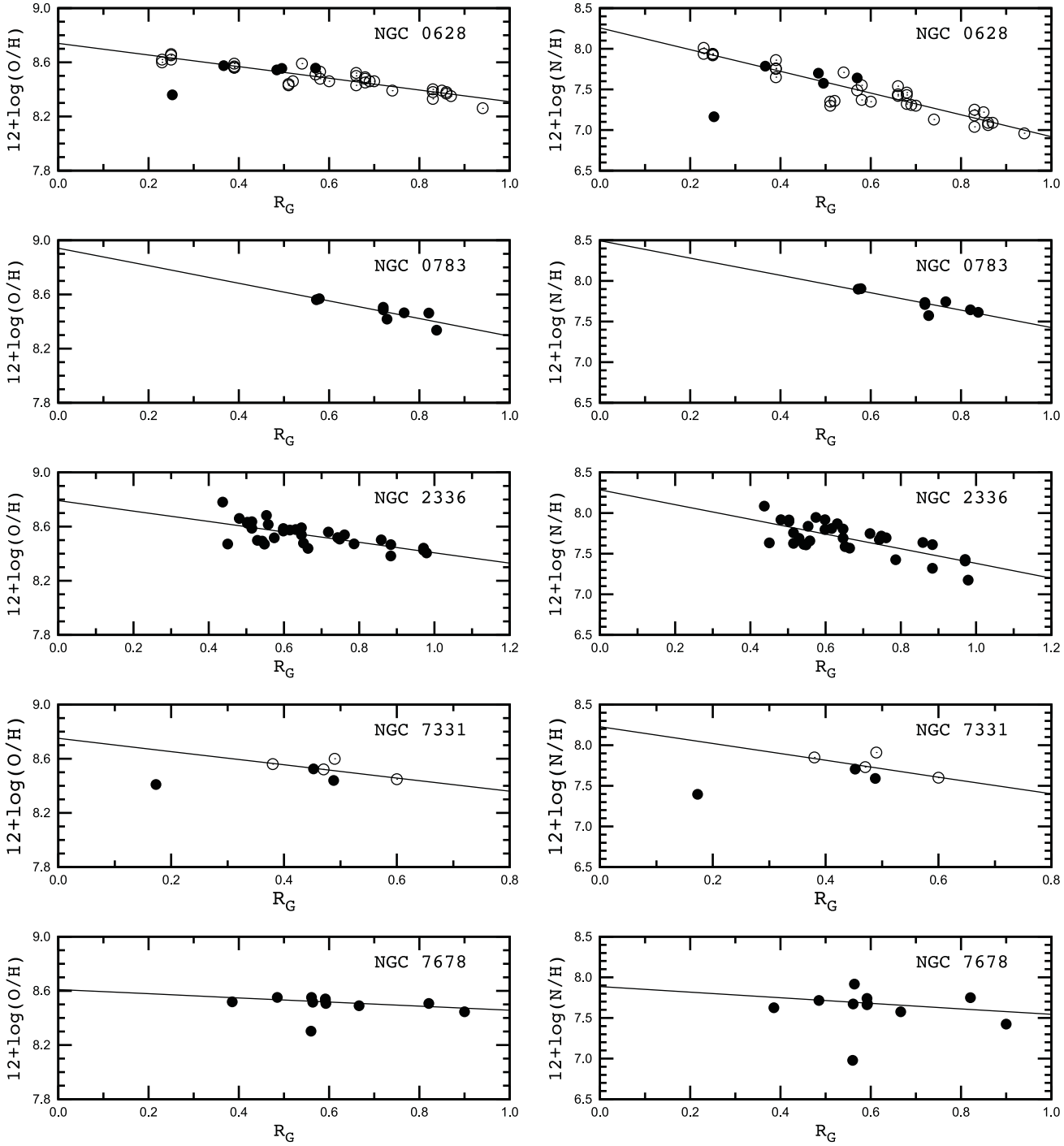

Figure 6. Radial distributions of oxygen abundances (left column) and nitrogen abundances (right column) in the discs of galaxies. Filled circles are abundances estimated from our observational data, open circles abundances based on the line measurements from the literature. The solid lines are best fits to these data points.

observations. Nevertheless, the abundance estimations in NGC 628 and NGC 7331 can be directly compared with previously published ones. First we estimated the oxygen and nitrogen abundances through the NS calibration, using previously published line measurements. Further, we plotted these estimations on the diagram of radial distributions of oxygen and nitrogen abundances in the discs of NGC 628 and NGC 7331, together with our abundance estimations.

The galactocentric distances were recomputed with the inclinations and position angles adopted here (Table 1).

Fig. 6 shows a good agreement in the radial abundance distributions in NGC 628 and NGC 7331 between H II regions observed in the present paper (filled circles) and H II regions observed previously (open circles).

The numerical values of the coefficients in equation (9) ($C_{O/H}$ and $12 + \log(O/H)_0$) and in equation (10) ($C_{N/H}$ and $12 + \log(N/H)_0$) have been derived through the least-squares method. Both our data and data from the literature are used. If there are data points that deviate significantly (more than 3σ) from the general trend, then these points were excluded in the derivation of the final relations. The obtained relations are presented in Fig. 6 by solid lines. Computed parameters of the radial distributions of oxygen and nitrogen abundances (the numerical values of the coefficients in equations 9 and 10) in the discs of galaxies NGC 628, NGC 783, NGC 2336, NGC 7331 and NGC 7678 are listed in Table 6.

3.4 Discussion

Examination of Fig. 6 shows that the radial distributions of the oxygen and nitrogen abundances in the discs of the considered galaxies are fitted well by a single linear expression within the optical isophotal radius. The variation of nitrogen abundance with galactocentric distance shows a larger amplitude in comparison to that of oxygen abundance and the differences in nitrogen abundance gradients between galaxies are larger than those in oxygen abundance gradients.

The luminosity–central metallicity diagram for spiral and irregular galaxies has been constructed by Pilyugin et al. (2007). The abundances of H II regions in that paper and here have been estimated through methods producing abundances that are in agreement with the abundance scale defined by the classic T_e method. Therefore the abundances obtained in these studies can be compared. Fig. 7 shows the luminosity–central metallicity diagram. The grey (blue) squares show the central abundances in the discs of spiral galaxies and abundances in irregular galaxies from Pilyugin et al. (2007). The dark (black) circles denote the central abundances in the discs of spiral galaxies from the present sample. The absolute blue magnitudes M_B are taken from the LEDA data base. Inspection of Fig. 7 shows that our sample of galaxies follows well the general trend in the luminosity–central metallicity diagram for spiral and irregular galaxies.

Table 6. Parameters of radial distributions of oxygen and nitrogen abundances in the discs of galaxies.

Galaxy	O/H centre[a]	O/H gradient[b]	N/H centre[a]	N/H gradient[b]
NGC 628	8.74 ± 0.02	-0.43 ± 0.03	8.26 ± 0.05	-1.34 ± 0.08
NGC 783	8.94 ± 0.12	-0.65 ± 0.16	8.49 ± 0.19	-1.07 ± 0.26
NGC 2336	8.79 ± 0.05	-0.38 ± 0.07	8.25 ± 0.10	-0.90 ± 0.15
NGC 7331	8.75 ± 0.18	-0.49 ± 0.36	8.23 ± 0.36	-1.03 ± 0.74
NGC 7678	8.61 ± 0.03	-0.15 ± 0.05	7.89 ± 0.17	-0.34 ± 0.27

[a]In units of $12 + \log(X/H)$.
[b]In units of dex/R_{25}.

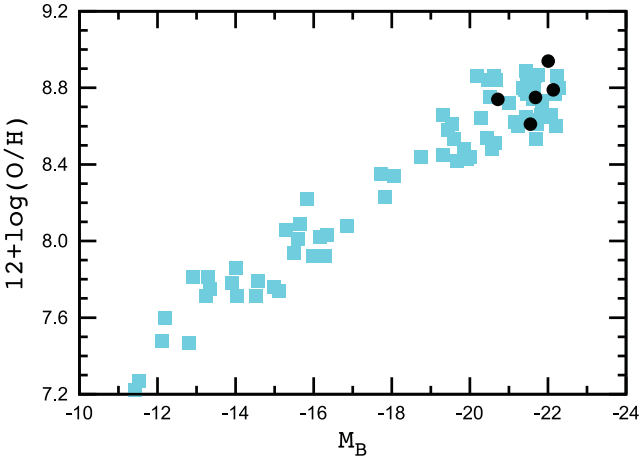

Figure 7. The luminosity–central metallicity diagram. The dark (black) circles denote the central abundances in the discs of spiral galaxies from the present sample. The grey (blue) squares show the central abundances in the discs of spiral galaxies and abundances in irregular galaxies from Pilyugin, Thuan & Vílchez (2007). (A colour version of this figure is available in the online version.)

4 CONCLUSIONS

The spectroscopic observations of H II regions in six spiral galaxies (NGC 628, NGC 783, NGC 2336, NGC 6217, NGC 7331 and NGC 7678) obtained with the 6-m telescope of the Special Astrophysical Observatory (SAO) of the Russian Academy of Sciences were carried out.

The oxygen and nitrogen abundances as well the electron temperatures in 50 H II regions are estimated using the recent version of the strong-line method (the NS calibration). The parameters of the radial distributions (the extrapolated central intercept value and the gradient) of the oxygen and nitrogen abundances in the discs of NGC 628, NGC 783, NGC 2336 and NGC 7678 are obtained. The oxygen and nitrogen abundances and their gradients in the discs of spiral galaxies NGC 783, NGC 2336 and NGC 7678 are estimated for the first time. The abundances for NGC 6217 are also found for the first time.

Galaxies from our sample follow well the general trend in the luminosity–central metallicity diagram for spiral and irregular galaxies.

ACKNOWLEDGMENTS

We are grateful to the referee for constructive comments. LSP acknowledges support from the Cosmomicrophysics project of the National Academy of Sciences of Ukraine. ASG is grateful to A.Y. Kniazev (South African Astronomical Observatory), L.V. Afanasiev and A.V. Moiseev (Special Astrophysical Observatory) for help and support during the observations in SAO and for fruitful discussion, and to A.V. Zasov and B.P. Artamonov (Sternberg Astronomical Institute) for useful discussions. The authors acknowledge the usage of the HyperLeda data base (http://leda.univ-lyon1.fr). This study was supported in part by the Russian Foundation for Basic Research (project nos 08–02–01323, 10–02–91338, and 12–02–00827). Results were based on observations collected with the 6-m telescope of the Special Astrophysical Observatory (SAO) of the Russian

Academy of Sciences (RAS), operated under the financial support of the Science Department of Russia (registration number 01–43).

REFERENCES

Afanasiev L. V., Moiseev A. V., 2005, Astron. Lett., 31, 193
Alloin D., Collin-Souffrin S., Joly M., Vigroux L., 1979, A&A, 78, 200
Artamonov B. P., Bruevich V. V., Gusev A. S., 1997, Astron. Rep., 41, 577
Artamonov B. P., Badan Yu. Yu., Bruyevich V. V., Gusev A. S., 1999, Astron. Rep., 43, 377
Baldwin J. A., Phillips M. M., Terlevich R., 1981, PASP, 93, 5
Belley J., Roy J.-R., 1992, ApJS, 78, 61
Bresolin F., Kennicutt R. C., Garnett D. R., 1999, ApJ, 510, 104
Bresolin F., Schaerer D., González Delgado R. M., Stasińska G., 2005, A&A, 441, 981
Bresolin F., Gieren W., Kudritzki R.-P., Pietrzyński G., Urbaneja M. A., Carraro G., 2009, ApJ, 700, 309
Bruevich V. V., Gusev A. S., Ezhkova O. V., Sakhibov F. Kh., Smirnov M. A., 2007, Astron. Rep., 51, 222
Chiappini V., Romano D., Matteucci F., 2003, MNRAS, 339, 63
Dinerstein H. L., 1990, in Thronson H. A., Jr, Shull J. M., eds, The Interstellar Medium in Galaxies. Kluwer, Dordrecht, p. 257
Dopita M. A., Evans I. N., 1986, ApJ, 307, 431
Dutil D. R., Roy J.-R., 1999, ApJ, 516, 62
Ellison S. L., Patton D. R., Simard L., McConnachie A. W., 2008, AJ, 135, 1877
Ferguson A. M. N., Gallagher J. S., Wyse R. F. G., 1998, AJ, 116, 673
Garnett D. R., 2002, ApJ, 581, 1019
Garnett D. R., Shields G. A., 1987, ApJ, 317, 82
Gusev A. S., 2006a, Astron. Rep., 50, 167
Gusev A. S., 2006b, Astron. Rep., 50, 182
Gusev A. S., Park M.-G., 2003, A&A, 410, 117
Gutiérrez L., Beckman J. E., 2010, ApJ, 710, L44
Henry R. B. C., Edmunds M. G., Köppen J., 2000, ApJ, 541, 660
Izotov Y. I., Thuan T. X., Lipovetsky V. A., 1994, ApJ, 435, 647
Kartasheva T. A., Chunakova N. M., 1978, Izv. SAO, 10, 44
Kauffmann G. et al., 2003, MNRAS, 346, 1055
Kennicutt R. C., 1984, ApJ, 287, 116
Kennicutt R. C., Bresolin F., Garnett D. R., 2003, ApJ, 591, 801
Kewley L. J., Dopita M. A., Sutherland R. S., Heisler C. A., Trevena J., 2001, ApJ, 556, 121
Liang Y. C., Yin S. Y., Hammer F., Deng L. C., Flores H., Zhang B., 2006, ApJ, 652, 257
López-Sánchez Á. R., Esteban C., 2010, A&A, 517, A85
Maeder A., 1992, A&A, 264, 105
Marcon-Uchida M. M., Matteucci F., Costa R. D. D., 2010, A&A, 520, A35
McCall M. L., Rybski P. M., Shields G. A., 1985, ApJS, 57, 1
Moustakas J., Kennicutt R. C., Jr, Tremonti C. A., Dale D. A., Smith J.-D. T., Calzetti D., 2010, ApJS, 190, 233
Oke J. B., 1990, AJ, 99, 1621
Osterbrock D. E., 1989, Astrophysics of gaseous nebulae and active galactic nuclei. University Science Books, Mill Valley, CA, p. 422
Pagel B. E. J., 1991, in Oberhummer H., ed., Nuclei in the Cosmos. Springer, Berlin, p. 89
Pagel B. E. J., 1997, Nucleosynthesis and Chemical Evolution of Galaxies. Cambridge Univ. Press, Cambridge, p. 392
Pagel B. E. J., Edmunds M. G., Blackwell D. E., Chun M. S., Smith G., 1979, MNRAS, 189, 95
Paturel G., Petit C., Prugniel Ph., Theureau G., Rousseau J., Brouty M., Dubois P., Cambresy L., 2003, A&A, 412, 45
Pettini M., Pagel B. E. J., 2004, MNRAS, 348, L59
Pilyugin L. S., 2000, A&A, 362, 325
Pilyugin L. S., 2001, A&A, 369, 594
Pilyugin L. S., Mattsson L., 2011, MNRAS, 412, 1145
Pilyugin L. S., Thuan T. X., 2005, ApJ, 631, 231
Pilyugin L. S., Thuan T. X., 2011, ApJ, 726, L23
Pilyugin L. S., Vílchez J. M., Contini T., 2004, A&A, 425, 849
Pilyugin L. S., Thuan T. X., Vílchez J. M., 2007, MNRAS, 376, 353
Pilyugin L. S., Vílchez J. M., Thuan T. X., 2010, ApJ, 720, 1738
Pilyugin L. S., Vílchez J. M., Mattsson L., Thuan T. X., 2012, MNRAS, 421, 1624
Rosales-Ortega F. F., Diaz A. I., Kennicutt R. C., Sanchez S. F., 2011, MNRAS, 415, 2439
Roy J.-R., Belley J., Dutil Y., Martin P., 1996, ApJ, 460, 294
Searle L., 1971, ApJ, 168, 327
Stasińska G., 2006, A&A, 454, L127
Storey P. J., Zeippen C. J., 2000, MNRAS, 312, 813
Thuan T. X., Pilyugin L. S., Zinchenko I. A., 2010, ApJ, 712, 1029
Tremonti C. A. et al., 2004, ApJ, 613, 898
van den Hoek L. B., Groenewegen M. A. T., 1997, A&AS, 123, 305
van Zee L., Salzer J. J., Haynes M. P., O'Donoghue A. A., Balonek T. J., 1998, AJ, 116, 2805
Vila Costas M. B., Edmunds M. G., 1992, MNRAS, 259, 121
Vilchez J. M., Esteban C., 1996, MNRAS, 280, 720
Zaritsky D., Kennicutt R. C., Huchra J. P., 1994, ApJ, 420, 87

This paper has been typeset from a TEX/LATEX file prepared by the author.